Society For Biomaterials

# Investigation of the cytotoxicity of aluminum oxide nanoparticles and nanowires and their localization in L929 fibroblasts and RAW264 macrophages

**Masanori Hashimoto, Jun-Ichi Sasaki, Satoshi Imazato**

Department of Biomaterials Science, Osaka University Graduate School of Dentistry, Suita, Osaka 565-0871, Japan

Received 3 July 2014; revised 9 December 2014; accepted 9 January 2015
Published online 26 February 2015 in Wiley Online Library (wileyonlinelibrary.com). DOI: 10.1002/jbm.b.33377

**Abstract:** The biological responses of aluminum oxide ($Al_2O_3$) nanoparticles (NPs) and nanowires (NWs) in cultured fibroblasts (L929) and macrophages (RAW264) were evaluated from their cytotoxicities and micromorphologic properties. Cultured cells were exposed to $Al_2O_3$NPs (13 nm diameter) and $Al_2O_3$NWs (2–6 × 200–400 nm). Cytotoxicity and genotoxicity were examined by immunostaining with fluorescence microscopy, and nanomaterial localization was studied by using scanning electron microscopy and transmission electron microscopy. The NPs were cytotoxic and genotoxic, whereas the NWs were not. The scanning electron microscopy images showed that the NPs aggregate more on the cell surface than do the NWs. The transmission electron microscopy images showed that the NPs were internalized into the vesicle and nuclei, for both cell types. In contrast, numerous solid NWs were observed as large aggregates in vesicles, but not in nuclei. Nuclear damage was confirmed by measuring cell viability and by immunostaining for NPs. The chemical changes induced by the NPs in the vesicles or cells may cause cell damage because of their large surface area per volume. The extent of NW entrapment was not sufficient to lower the viability of either cell type. © 2015 Wiley Periodicals, Inc. J Biomed Mater Res Part B: Appl Biomater, 104B: 241–252, 2016.

**Key Words:** aluminum oxide nanoparticle, aluminum oxide nanowire, L929, RAW264, cytotoxicity

**How to cite this article**: Hashimoto M, Sasaki J-I, Imazato S. 2016. Investigation of the cytotoxicity of aluminum oxide nanoparticles and nanowires and their localization in L929 fibroblasts and RAW264 macrophages. J Biomed Mater Res Part B 2016:104B:241–252.

## INTRODUCTION

Nanoscale materials are currently being developed for a wide range of applications, including in industry, military, and medicine, by virtue of their special size-dependent properties. Previous studies have shown that their biological reactivity depends on the length and aspect ratio of the nanorods and nanowires (NWs).[1–4] Nanomaterials of different shapes and sizes (nanoparticle (NP), nanorod, and NW) are promising tools for cell imaging, tracking, and sensing for diagnostic or therapeutic applications.[5] Although implementation of nanomaterials requires them to possess a high degree of biosafety, the effects of nanomaterials on living cells, tissues, or organs has not been fully evaluated.

Asbestos is a well-known material that induces chronic granulomatous inflammation because of their engulfment by macrophages as a result of their special morphology, which includes their high aspect ratio. Moreover, the high aspect ratio of carbon nanotubes with shapes similar to that of asbestos induces a proinflammatory response in human primary macrophages.[6] Therefore, there is a possibility that newly developed nanomaterials with unique shapes may induce some unknown and undesirable biological responses inside cells or organs.

Aluminum oxide ($Al_2O_3$) NP is one of the most popular nanomaterials used in coatings, abrasives, and additives in industrial composite. Based on these extensive commercial applications, they have drawn considerable attention as potential environmental pollutants. It is well known that aluminum possesses low acute cytotoxicity, but chronic exposure induces neurologic disorders such as Alzheimer's disease. Additionally, $Al_2O_3$ is used as an orthopedic material[7] or restorative material in medicine and dentistry.[8,9] Clinical applications of $Al_2O_3$ nanomaterials will undoubtedly increase in the future. Many reports have shown that aluminum NPs are relatively safe, compared with other metal NPs. However, the nanotoxicity of $Al_2O_3$NPs has not been studied in depth compared with that of AuNPs and AgNPs. Moreover, there is very little information on the potential cytotoxicity of $Al_2O_3$ NPs and NWs.

The objective of this study was to evaluate the effects of $Al_2O_3$NPs (particle size: 13 nm) and $Al_2O_3$NWs (particle size: 2–6 × 200–400 nm) on cultured L929 and RAW264

**Correspondence to:** M. Hashimoto; e-mail: masanori-h@mue.biglobe.ne.jp
Contract grant sponsor: Grants-in-Aid for Scientific Research from the Japan Society for the Promotion of Science (JSPS); contract grant numbers: 26462953 and 24659846

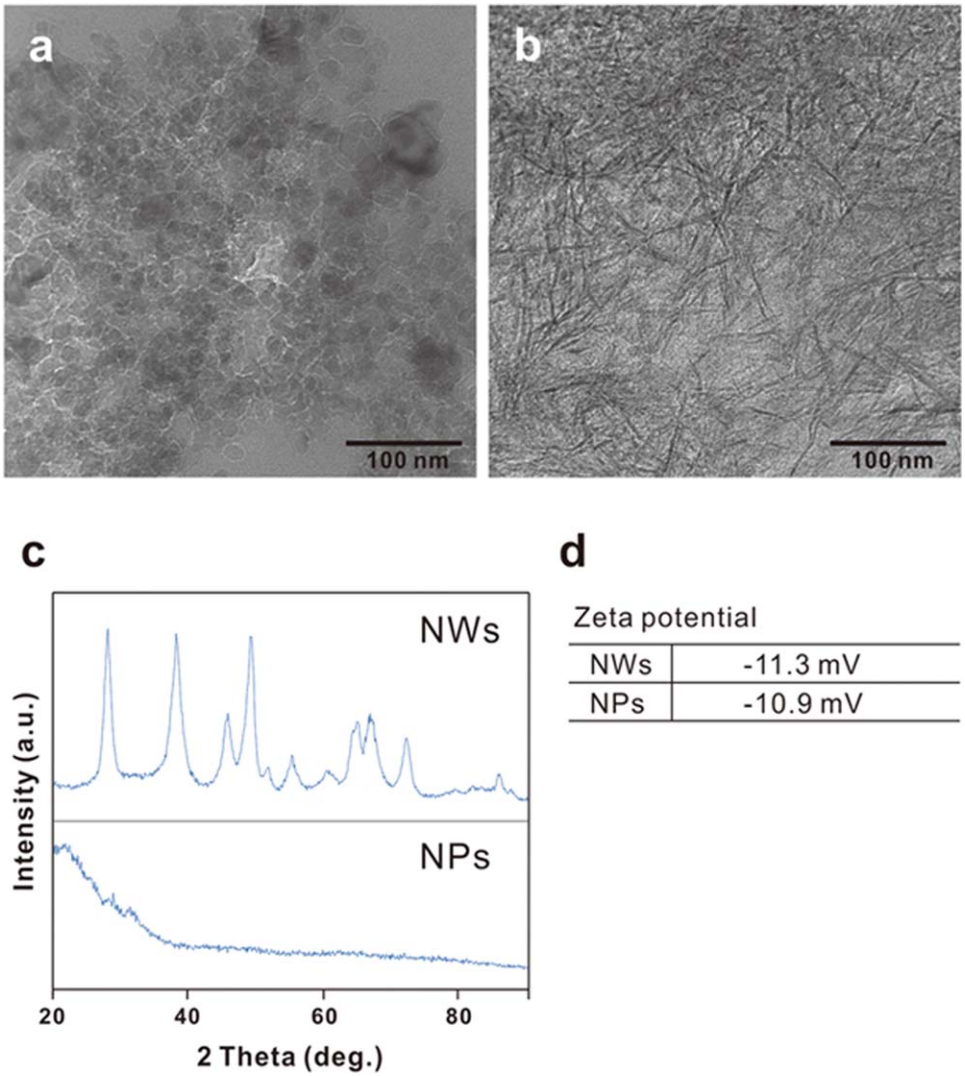


**FIGURE 1**. TEM images of NPs (a) and NWs (b). The crystal phases of NPs and NWs were examined by XRD (c). The zeta-potential of NPs and NWs are shown in (d).

cells using cytotoxicity measurements, immunostaining with confocal microscopy, and micromorphological analysis of the internalization of NPs and NWs using scanning electron microscopy (SEM) and transmission electron microscopy (TEM).

## MATERIALS AND METHODS

### Test materials

$Al_2O_3$ NP (13 nm in diameter) and NW (2–6 $\times$ 200–400 nm) (Sigma-Aldrich, St. Louis, MO) were used in this study. Epoxy resin-embedded NPs or NWs were prepared for TEM. The shape of test materials was observed using transmission electron microscope (H-7100, Hitachi, Tokyo, Japan). The crystallinity of the samples was characterized by X-ray diffraction (XRD; Rint 2100, Rigaku, Tokyo, Japan). The surface charge of the samples was measured by a zeta-potential analyzer (Zetasizer Nano-ZS, Malvern Instruments, Worcestershire, UK).

### Cell culture and preparation of the conditioned medium

The L929 fibroblasts and RAW264 murine macrophage cells (Riken Biosource Center Cell Bank, Tsukuba, Japan) were cultured at 37 °C in α-minimal essential medium (Wako Chemical, Tokyo, Japan) containing 10% (v/v) fetal bovine serum (Japan Bio Serum, Hiroshima, Japan), penicillin, and streptomycin (Anti-Anti, Gibco, Grand Island, NY) in a humidified atmosphere of 5% $CO_2$ in air.

### Suspension preparation and centrifugation process

Two test processes were carried out: (1) direct exposure of the test materials to cells and (2) exposure of the NP or NW supernatant suspensions to cells. Cells were seeded in Falcon 96-well plates (Corning, Corning, NY) at a density of $1 \times 10^4$ cells per well with 200 μL of medium. After 72 h of culturing, the medium was removed, and 200 μL of medium containing three different NP and NW concentrations (50, 100, or 200 μg/mL) was added in the direct

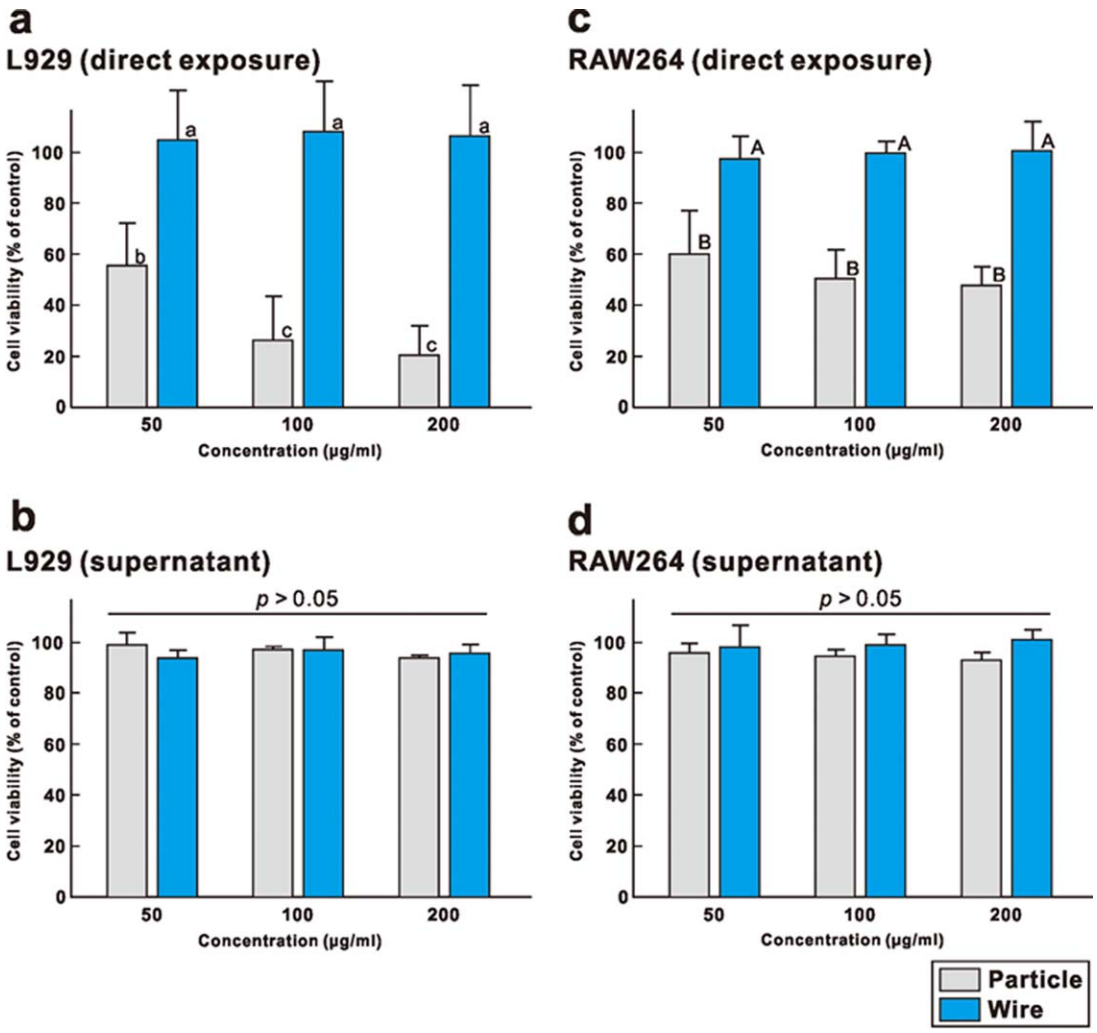


**FIGURE 2**. Cell viability of L929 and RAW264 cells cultured in control medium, suspensions, or supernatants of 50, 100, and 200 μg/mL of test materials. The optical density values were calculated as a percentage of that of the control group. Groups that were significantly different are indicated by different letters ($n = 5$, $p < 0.05$).

exposure group. Cells that had not been treated using the test materials were used as control. The stock solution was mixed using a vortex and then sonicated for 10 min to reduce agglomeration of the NPs and NWs. The test material-exposed cells were subsequently incubated for a further 24 h. For exposure of the supernatant group, the centrifugation of NPs or NWs suspensions (24 h exposure) was carried out at 1000*g* for 10 min using a centrifuge (LC-122, Tomy Seiko, Tokyo, Japan) to remove any suspended materials. After centrifugation, the supernatant was collected and added to the 72 h cultured cells. The supernatant exposed cells were subsequently incubated for 24 h.

### Cell viability

The cell viability was measured using a WST-8 assay (CCK-8, Dojindo, Kumamoto, Japan). The cells were incubated in medium in 96-well plates ($1 \times 10^4$ cells/200 μL medium/well) for 72 h and followed by a 24 h exposure to the NPs, NWs, or supernatant. The medium was then aspirated out, and the cells were washed twice using phosphate-buffered saline. The medium and WST-8 test solution were then added, and the plate was incubated at 37 °C for 1 h. After 1 h, the cell supernatant was placed in a new 96-well plate, and the absorbance at 450 nm was measured using a microplate reader (1420 Multilabel Counter, PerkinElmer, Waltham, MA). The test medium was carefully transferred to a new 96-well plate to avoid contamination of the NPs or NWs in the medium. Blank and medium controls (medium containing NPs or NWs without cells) were treated identically.

### Lactate dehydrogenase release

Lactate dehydrogenase (LDH) was measured (LDH Cytotoxicity Detection kit, Takara, Tokyo, Japan) to evaluate the plasma membrane integrity. The amount of the LDH released by the cells (and subsequently found in the culture supernatant) was determined using a coupled enzymatic assay involving the conversion of a tetrazolium salt into a formazan product. The cells were incubated in medium in

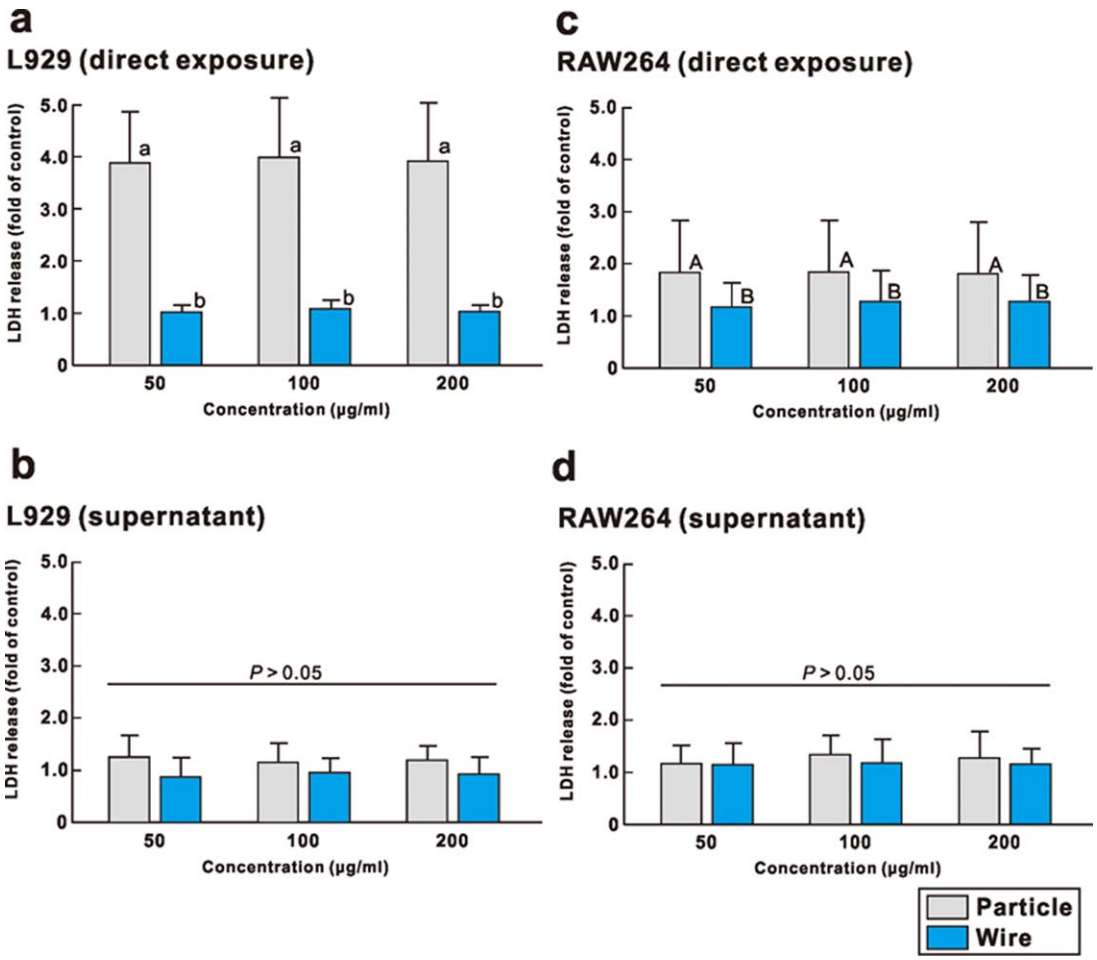


**FIGURE 3**. LDH release of L929 and RAW264 cells cultured in control medium, suspensions, or supernatants of 50, 100, and 200 μg/mL of test materials. The optical density was calculated as a percentage of that of the control group. Groups that were significantly different are indicated by different letters ($n = 4$, $p < 0.05$).

96-well plates for 72 h as previously described, and then incubated for 24 h with various concentrations of Ag-NPs freshly dispersed in culture medium that did not contain fetal bovine serum. Subsequently, 120 μL of each supernatant was transferred into a 1.5-mL tube and centrifuged for 10 min. After centrifugation, the supernatant of each sample (100 μL) was then carefully transferred to a well in a new 96-well plate, and 100 μL of LDH reaction solution was added. The plates were incubated for 30 min, after which their colorimetric absorbance was recorded at 490 nm using a microplate reader (1420 Multilabel Counter).

### Immunocytochemical staining

Nuclear morphology and distribution were investigated by immunocytochemistry. An established biomarker for genomic instability was used to evaluate the susceptibility of cells to NP-induced chromosomal damage (micronuclei and misshapen nuclei) and structural damage. After exposure to NPs, the cells were incubated with Hoechst 33342 (Invitrogen, Carlsbad, CA) and rhodamine phalloidin (Invitrogen) for 30 min. The cells, their nucleus, and F-actin were observed using fluorescence microscope (TS1200-E, Nikon, Tokyo, Japan).

### Analysis of changes in nuclear shape

Genotoxicity was evaluated by measuring the frequency of the occurrence of misshapen nuclei (micronuclei and deformed nuclei), which would indicate chromosomal damage, induced by NPs or NWs. After exposure to the nanomaterials, the cells were incubated with Hoechst 33342 (Dojindo) for 30 min. The number of cells exhibiting misshapen nuclei was counted, with over 150 nuclei analyzed per treatment time point and all analyses performed in four identical trials. The number of nuclei was scored in the fluorescence microscopy images (TS1200-E).

### Morphological analysis

A phase-contrast inverted microscope (Eclipse TS2000E, Nikon), connected to a digital camera was used to capture optical images of the test materials or cells. For SEM and TEM analyses, the cells incubated with and without NPs were washed using phosphate-buffered saline and fixed with 2.5% glutaraldehyde for 24 h. The cells were then postfixed in 1% osmium tetroxide for 1 h and washed and dehydrated in graded concentrations of ethanol (50, 60, 70, 80, 90, and 100%) and hexamethyl-disilazane (Wako). For SEM analysis, the specimens were sputter-coated with gold and observed

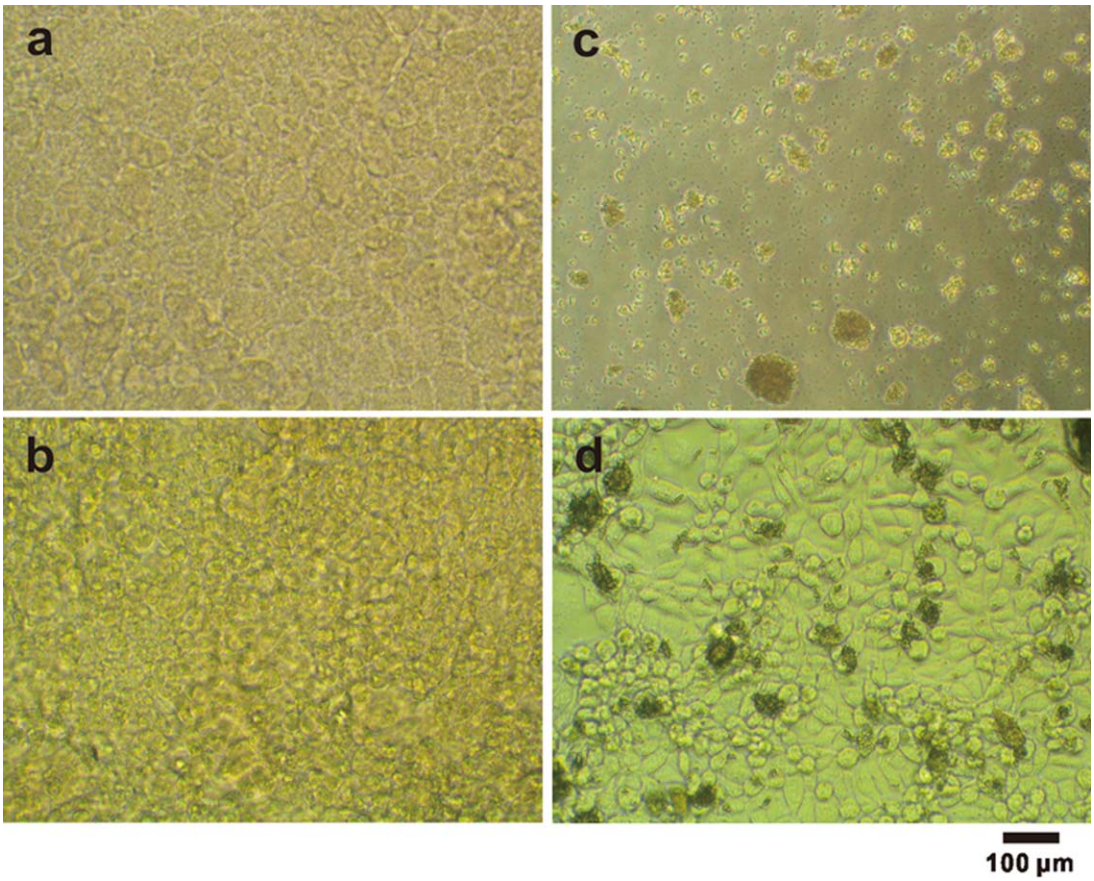


**FIGURE 4**. Optical microscopic images of NPs on a dish without cells (a) and with cells (b), and NWs on a dish without cells (c) and with cells (d). The NPs and NWs were at 200 μg/mL. The aggregates of NWs were clearly visible on the culture dish (c) or on the RAW264 cells (d).

using scanning electron microscope (JSM-6390BU, JEOL, Tokyo, Japan). For TEM analysis, the cell specimens were infiltrated with, and embedded in, epoxy resin (EPON 812, TAAB, West Berkshire, UK). Subsequently, ultrathin sections (90 nm) were cut from the epoxy-embedded specimens using a diamond knife on a microtome (Sorvall MT-5000, Du Pont, Palo Alto, CA). The sections were collected on copper grids and observed under transmission electron microscope.

### Statistics

Independent experiments were conducted, and the results were expressed as the mean ± standard deviation ($n = 5$ for WST-8 assay and $n = 4$ for LDH release assay and genotoxic analysis of nuclear shape). Analysis of variance was used to compare the mean values for the control and treatment groups ($p < 0.05$ for each).

## RESULTS

### NP characterization and cell viability

The spherical shapes of the NPs and wire shape of the NWs were observed in the TEM images [Figure 1(a,b)]. The crystallinity was amorphous for NPs and crystal structures were obtained for NWs by XRD [Figure 1(c)]. The zeta-potential of the NPs and NWs was −10.9 and −11.3 mV, respectively [Figure 1(d)].

### Cell viability

The effects of the NPs and NWs on the cell viability (WST-8 assay) are illustrated in Figure 2. The cell viability was significantly reduced after NP exposure at all concentrations in both cells in the direct exposure group [$p < 0.05$; Figure 2(a,c)]. However, no significant changes were found from the NW exposure [$p > 0.05$; Figure 2(a,c)]. For the supernatant exposure group, no significant differences were observed for all concentrations ($p > 0.05$) in both cells [Figure 2(b,d)].

### LDH release assay

The effects of the NPs and NWs on the LDH release (LDH assay) are illustrated in Figure 3. The LDH release significantly increased after direct exposure of L929 and RAW264 cells to NPs compared with that of the control groups ($p < 0.05$). However, the LDH release upon exposure to NWs was not significantly different from that of the control, for either the supernatant group or the direct exposure group of NWs ($p > 0.05$).

### Optical microscopic images

Figure 4 shows the optical microscopic images of test materials and cells in the well of 96-well multiwell plates. The NPs were dispersed on the bottom of culture plate [Figure 4(a)] or on the RAW264 cells [Figure 4(b)]. Some aggregates of

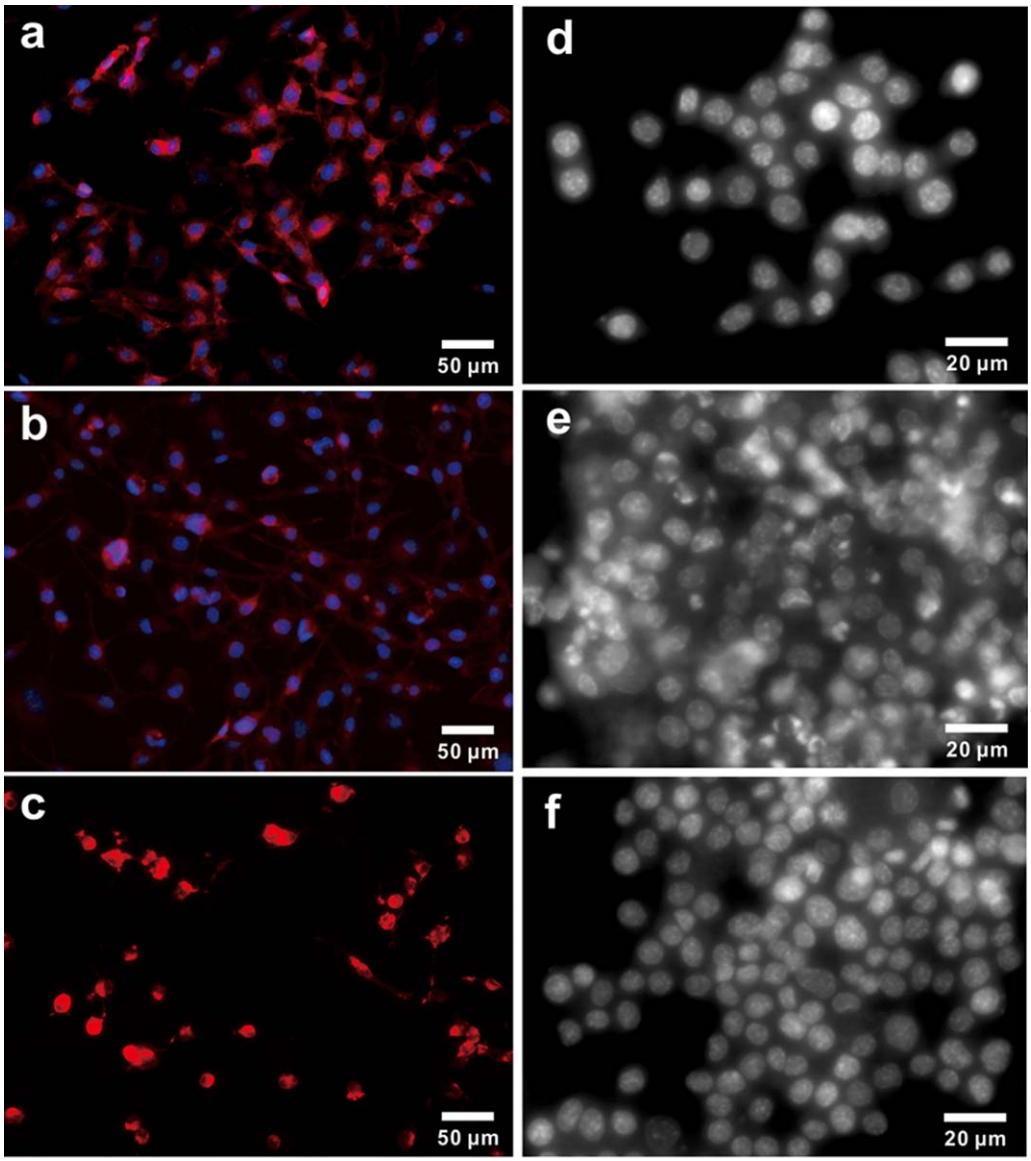


**FIGURE 5**. Fluorescence microscopy images (blue: Hoechst33342 and red: rhodamine phalloidin) of: (a) Normal nuclei of L929 cells. (b) Exposure of L929 cells to 200 μg/mL NW. (c) Exposure of L929 cells to 200 μg/mL NP. Cell nuclei of RAW264 stained with Hoechst 33342 (white) (d: control, e: 100 μg/mL NP exposure, and f: 200 μg/mL NW exposure). Nuclear deformation was observed in the cells exposed to NP (c and e).

NWs were observed on the bottom of the culture plate or on the cells [Figure 4(c,d)]. The same results were obtained for the incubations with L929 fibroblasts (data not shown).

### Immunocytochemical staining

Figure 5 shows the morphological changes observed by immunostaining coupled with fluorescence microscopy after exposure to NPs or NWs. The cell structural damage was evident after rhodamine phalloidin staining [Figure 5(c)], and nucleus damage as shown by misshapen nuclei or micronuclei [Figure 5(e)] was clearly observed after NP exposure. The structural and nuclear damage of the control and NW exposure groups were lower compared with that in cells exposed to NP. Additionally, no morphological changes were evident between the control and the supernatant exposed groups (data not shown). Identical results were obtained regardless of the cell type.

### Analysis of changes in nuclear shape

Figure 6 shows the frequency of the occurrence (%) of misshapen nuclei. The frequency of misshapen nuclei from the direct exposure group (NPs) is significantly greater than that of the control [$p < 0.05$; Figure 6(a,c)]. Significant differences were found in the NW exposure group, compared with the control ($p < 0.05$), for L929 cells, but not RAW264 ($p > 0.05$). However, no significant differences were found in the frequency of occurrence of micronuclei or deformed nuclei in the supernatant group [$p > 0.05$; Figure 6(b,d)].

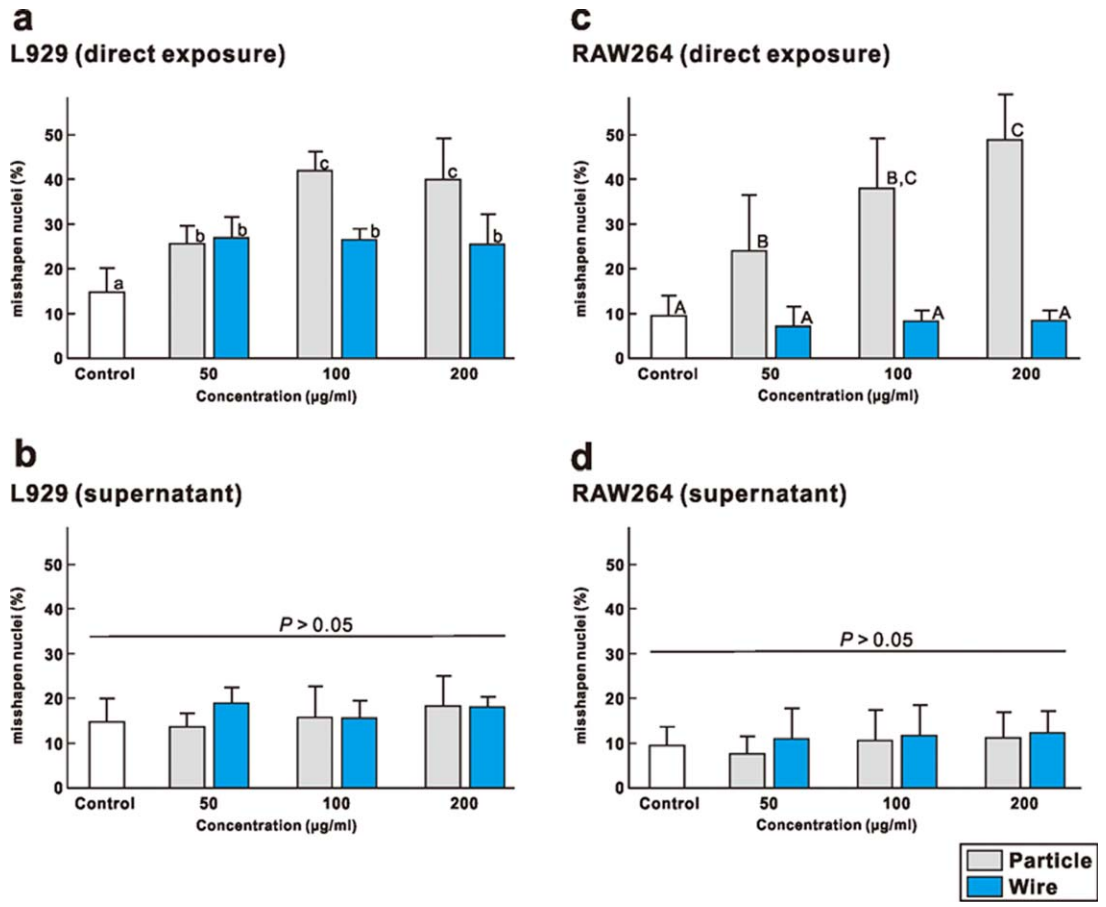


**FIGURE 6**. Analysis of misshapen nuclei of L929 and RAW264 cells cultured in control medium, suspensions, or supernatants of 50, 100, and 200 μg/mL of test materials. The number of misshapen and normal nuclei was counted in fluorescence microscopy images and then the frequency of misshapen nuclei was expressed as percentage. Groups that were significantly different are indicated by different letters ($n = 4$, $p < 0.05$).

### SEM images

Figure 7 shows the SEM images of the cells [Figure 7(a,b): RAW264 and Figure 7(c,d): L929] treated with NPs [Figure 7(a,c)] and WPs [Figure 7(b,d)]. Small particles and their aggregates were observed on the cell surface of the NP group [Figure 7(a,c)]. The amount of NW surface aggregates was greater compared with the number of NP surface aggregates [Figure 7(b,d)].

### TEM images

Figure 8 shows the TEM images of L929 cells exposed to NPs [Figure 8(a–c)] and NWs [Figure 8(d–f)]. Numerous NPs were localized around the cell [Figure 8(a,b)] and partially inside the cell [Figure 8(b)]. The internalized $Al_2O_3$NPs were mainly observed in the vesicles of the cells treated with either NPs or NWs. Occasionally, some NPs were observed in the nuclei [Figure 8(c)]. Most NWs aggregated in the vesicles, not in the nuclei. The cells maintained their size and shape compared with the unexposed cells (control).

Figure 9 shows the TEM images of RAW264 cells exposed to NPs [Figure 9(a–c)] and NWs [Figure 9(d–f)]. The internalized $Al_2O_3$NPs were mainly observed in vesicles of the cells treated with either NPs or NWs. As shown in Figure 9(b), the NPs were localized in the cytoplasm. Some particles were observed in the nuclei [Figure 9(b)]; however, this was not common. Most NWs were observed in vesicles as large aggregates, but not in nuclei. In some cases, the cells were enlarged by lysosomal expansions because of the process of NW digestion [Figure 9(d)]. Figure 9(e,f) shows the endocytosis of NW aggregates into the cell.

## DISCUSSION

As discussed in several reviews,[10–12] the cytotoxic effects of nanomaterials on cells, organs, and the human body have not yet been fully shown. Moreover, comprehensive cytotoxicity data for $Al_2O_3$NPs and $Al_2O_3$NWs are even more scarce compared with data for other nanomaterials composed of gold, silver, or carbon. L929 and RAW264 cells are some of the commonly used cells in NPs research. Generally, RAW264 cells are more sensitive to cytotoxic compounds because being macrophages, they have a greater tendency toward endocytosis. However, the WST-8 assay showed that L929 cells experienced more cytotoxic damage than the RAW264 cells (Figure 2). Additionally, endocytosis of NPs and NWs clearly occurred in L929 cells, and the extent of

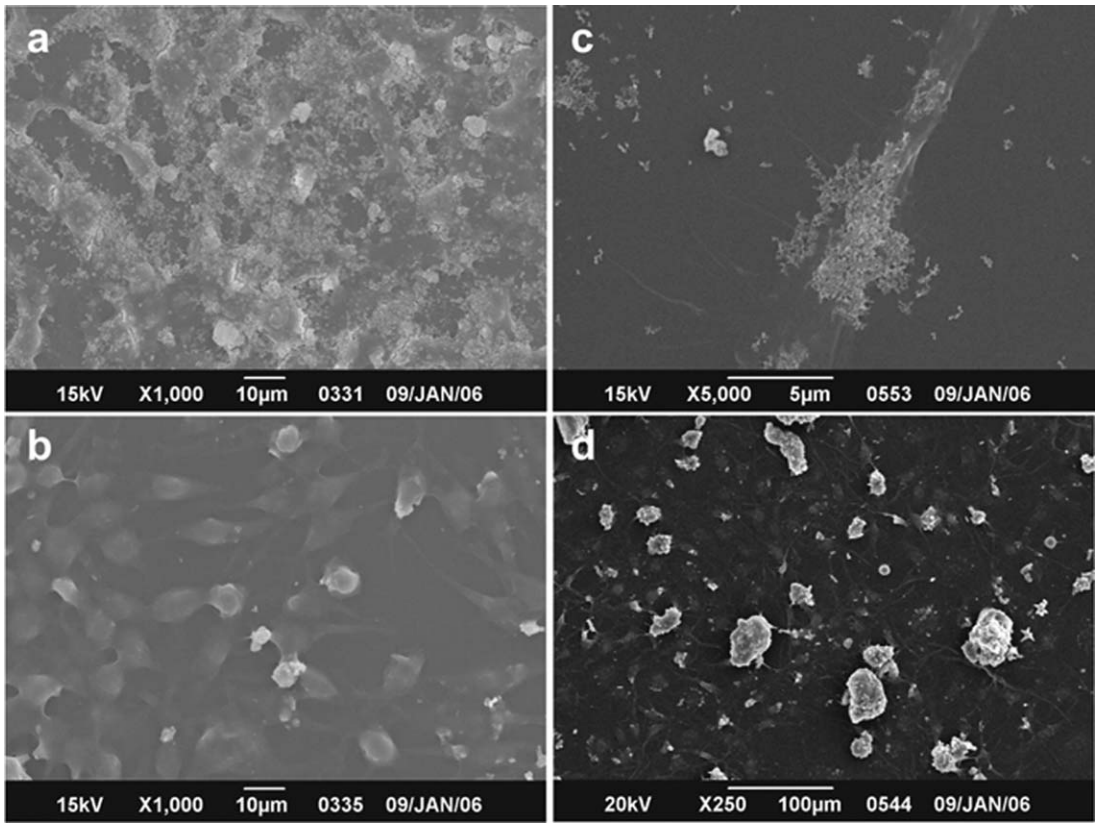


**FIGURE 7**. SEM images of cells exposed to NPs (a: RAW264 and c: L929) and NWs (b: RAW264 and d: L929) at concentrations of 100 μg/mL (a, b, and c) and 200 μg/mL (d).

engulfment of both materials seems to be the same in both cells from the micromorphological images obtained by TEM. The rate of LDH release (fold of control) from L929 was greater than that of RAW264 (NP direct exposure group) [Figure 3(a,c)]. Analyzing the occurrence of misshapen nuclei to determine genotoxicity showed that the NWs also damaged the nuclei of L929 cells [Figure 6(a)]. It is possible that the frequency of misshapen nuclei also reflects damage to the cell structure indicated by the WST-8 assay for cytotoxicity. Based on these results, we speculate that the L929 cells undergo much greater damage compared with RAW264 upon nanomaterial exposure, but this speculation should be reexamined under various test conditions. A recent study has shown the biocompatibility of $SiC/SiO_2$ NWs according to a cell viability assay (A549, HuDe, MCF-7, and THP-1 cells).[13] When germanium NWs were applied to L929 cells, an increase in cell proliferation was recorded using MTT and WST-1 assays and by quantifying the number of cells.[14] In contrast, another report has demonstrated that β-SiC NWs induce apoptosis due to oxidative stress in MC3T3-E1 cells after 48 h exposure to NWs, even though their cell viability remains high after 24 h exposure (MTT assay).[15] In the present study, direct exposure of L929 cells to NWs yielded differing results for cytotoxicity and genotoxicity. Therefore, further research is needed to examine and compare the various tests.

In this study, we directly observed the engulfment of NW aggregates from the surface of cells by TEM [Figure 9(e,f)]. This morphological phase of internalization was observed for both the macrophage (RAW264) and fibroblast (L929) cells. Additionally, SEM and optical microscopic images showed that many NWs aggregates were localized on the cell surface despite the fact that the aggregates were sporadic per unit area (Figures 4 and 7). The individual NWs were clearly observed as aggregates by TEM [Figure 8(f)]. However, localization of a single NW is difficult to observe in cells, which meant many NWs were directly engulfed by cells as aggregates. In previous studies, the extent of Al-NP agglomeration increased as the particle sizes increased, suggesting that the Al-NPs easily aggregated at high concentrations, in saline or cell culture medium.[16,17] These tendencies were observed for both nanomaterials tested in this study, especially for the NWs in culture medium in the presence and absence of cells.

NP and NW toxicity is generally proportional to the amount of ions in the test medium. Although no measurements were conducted to determine the amount of released ions in the test mediums, the released fraction of materials was enough to induce cytotoxic and genotoxic effects under the test conditions. An additional experiment with the supernatant suggested that the observed cytotoxic effects were likely caused by the intercellular NPs rather than the

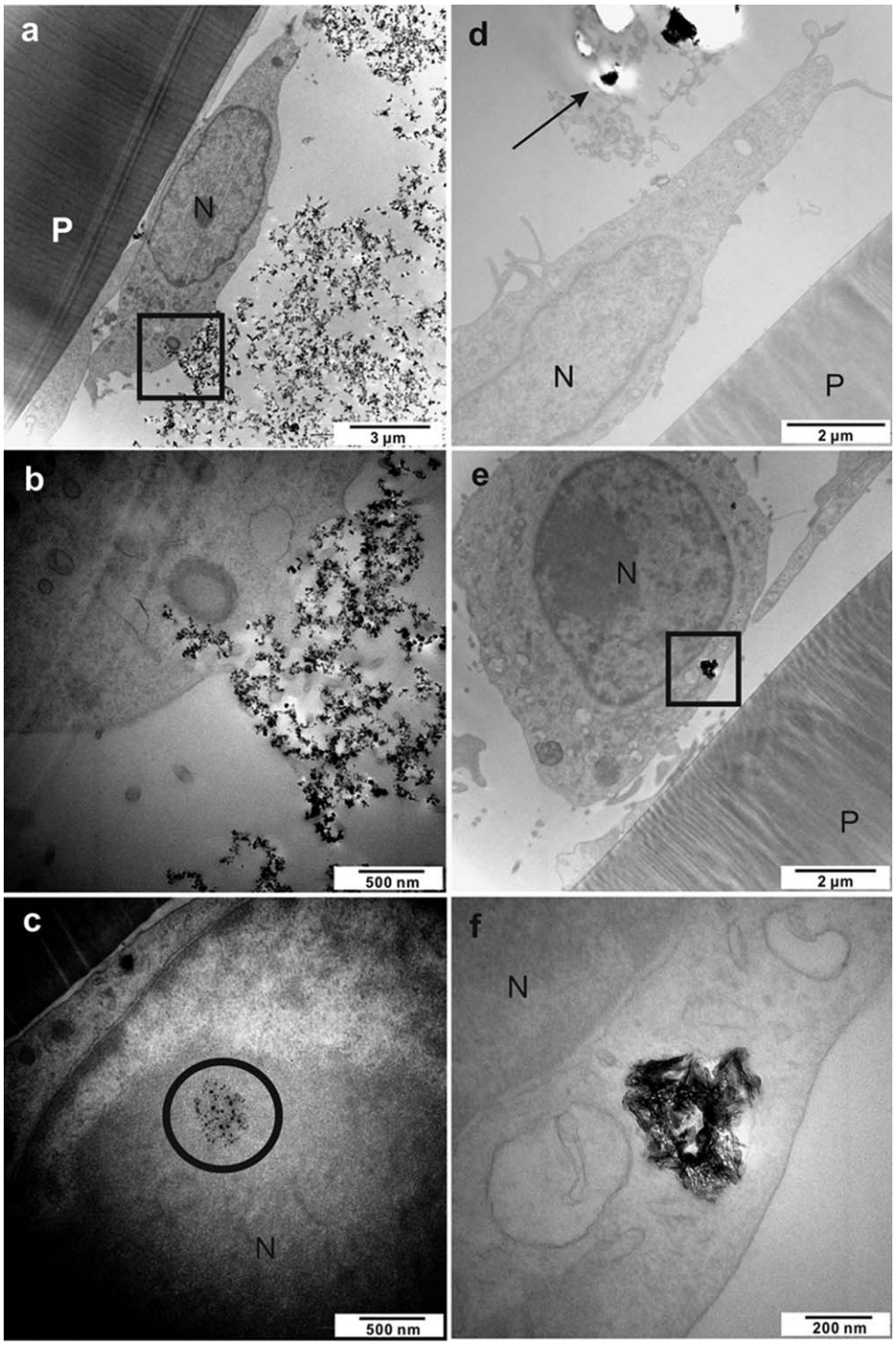


**FIGURE 8**. TEM micrographs of L929 cells incubated with NPs (a, b, and c: 200 μg/mL) and NWs (d, e, and f: 100 μg/mL). The particles were observed to be localized around the cell and in the cytoplasm (b) and nuclei (c: circle). The NPs tended to agglomerate inside the cells, but not in nuclei (d–f). The NWs were observed in vesicles, most likely in lysosomes. The boxed sections in (a) and (e) are shown at higher magnifications in (b) and (f). Black arrow indicates aggregates of NWs. N: nuclei, P: culture plate.

released ions. The results of this study suggest that material size and surface area play important roles in the observed cytotoxicity, but these effects are generated in the cells (Trojan horse-type effects), not by the generated ions found in the medium. Based on many reports that smaller particles result in more cytotoxicity compared with larger ones (size effects),[18–20] the high toxicity of NPs may primarily be as a result of their large surface area-to-volume ratio. The toxicity confirmed by the WST-8 assay is in accordance with the obtained genotoxic data and the nuclei deformation

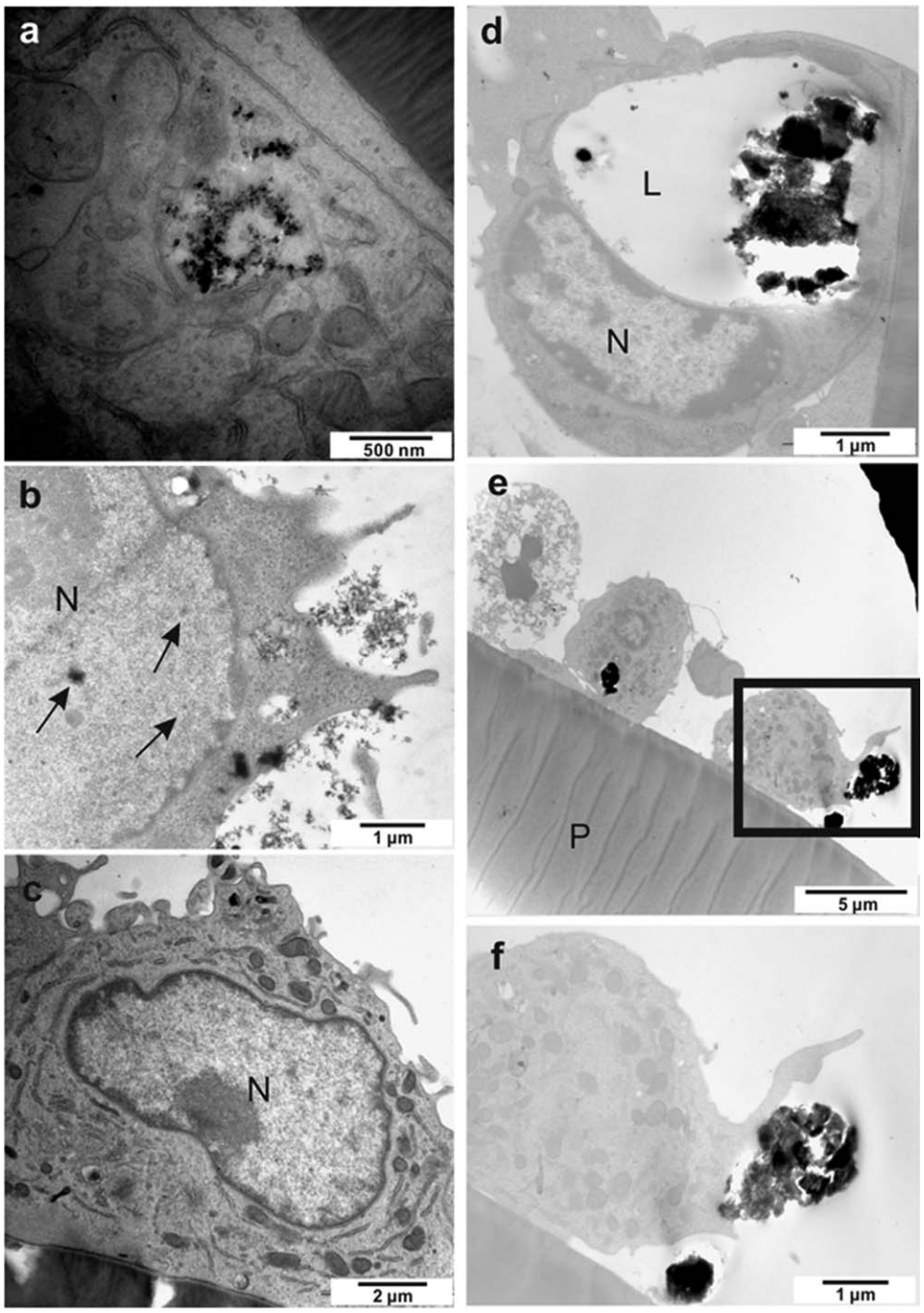


**FIGURE 9**. TEM micrographs of RAW264 cells incubated with various concentrations of NPs (a and b: 200 μg/mL) and (c: 100 μg/mL). The localization of the particles was observed in the cytoplasm (b). TEM micrographs of RAW264 cells incubated with 200 μg/mL of NW dispersions (d, e, and f). The wires tended to agglomerate in micron-sized groups inside the larger lysosomes (c and e). However, the NWs were found in lysosomes, not in the nuclei. The beginning step of endocytosis is shown in (f). The boxed section in (e) is shown at higher magnification in (f). Black arrows indicate NPs. N: nuclei, L: lysosome, P: culture plate.

observed by immunostaining for both NPs and NWs as a result of direct exposure and from the supernatant (except for the genotoxic analysis of direct exposure group of L929; Figure 5).

NPs degraded in the acidic environment of lysosomes (pH = 5.5), resulting in the release of ions from the core metals as toxic substances.[21,22] The intercellular release of free ions generates radicals and ROS in the intercellular environment. A recent report has shown by TEM that cells were able to degrade iron oxide NWs into smaller parts (shorter than the initial length).[20] Another study has shown the intercellular changes in morphology (STEM) and chemistry (EDX) of AgNWs from 1 h to 7 days of incubation.[3] Moreover, some reports have detailed the effect of

intracellular solubility of NPs on cytotoxicity.[3,20,23–25] From this study, we cannot distinguish the length or size distribution of the internalized NWs or NPs, or the time required for degradation of the NPs or NWs. Further research is required to examine the internal morphological changes induced by incubation with NPs or NWs for longer culture periods.

The NP and NW cytotoxicity is also influenced by their core composition and outer coatings. The toxic ions may leach out of the NP or wire when the outer coatings deteriorate or in the absence of coating agents.[25,26] Although no clear mechanism have been elucidated to account for the leaching, this may be accelerated in the intercellular environment, compared with water or test medium. Compared with silver, silica, or carbon nanomaterials, the toxic effects of aluminum nanomaterials are mild and are, thus, considered to be a safe material.[27–29] However, moderate cytotoxic and genotoxic effects were observed in this study for the aluminum NPs. Because the NPs and NWs used in this study were not coated, ions directly released from the core aluminum, and the materials were more cytotoxic compared with surface-coated nanomaterials or other examples of aluminum nanomaterials in the literature.[27–29]

Generally, if the nanomaterials are attached to the cell membrane, the cell membrane would be disrupted, resulting in interference of cellular activities. The degree of direct contact that occurs between a specific type of nanomaterial and cell membranes will vary depending on the nanomaterial structure as they may be single-walled, multiwalled, or have a dispersed structure or exist as aggregates.[30,31] This, in turn, impacts the induced toxicity. In SEM images, numerous NPs were deposited on the monolayer cell surfaces [Figure 7(a)]; however, many NPs did not make direct contact with the cells, as shown in the TEM image [Figure 8(a)]. Further studies are required to examine the interactions between the cell membranes and the nanomaterials and how that influences the downstream biological responses. Although the surface charges of NPs and NWs are almost the same [Figure 1(d)], variations in the amorphous phase or crystal structure between the NPs and NWs [Figure 1(c)] may also explain the observed differences in their cytotoxicity. Different cytotoxic effects were observed for anatase and rutile $TiO_2$ particles, and for crystalline silica compared with amorphous silica particles.[32]

The distribution of NPs and NWs in cells was identified using TEM. In Figures 8 and 9, the NPs were clearly visible as large aggregates on the inside and outside of both cells. The most frequent configuration observed was that of the NPs localized in the vesicles, with less in the nuclei or the cytoplasm. No NWs were found in the nuclei. It is difficult to observe the internalization of NPs into nuclei even by TEM because the electron density of aluminum nanomaterial is low compared with other metal NPs (i.e., silver or gold NPs). The nuclei localization of NPs was sporadic in TEM images, likely because the nuclei uptake of NPs was thought to be very limited. Some reports have shown that the phenomenon of nuclei NP penetration is size dependent, whereas we speculate that smaller NP (below 10 nm diameter) may be able to penetrate the nuclei pore.[33,34] The 12-nm-diameter NPs (including those without coating used in this study) invade the nuclei of the cells, and then induce irreversible cytotoxic and genotoxic cell damage. However, based on these investigations, NWs are a relatively safe material for administration to living cells, compared with NPs.

## CONCLUSION

The WST-8 assay and immunostaining showed that direct exposure to NPs induced cell death and nuclear damage in both cell types. Conversely, the NWs were not cytotoxic and did not damage the cellular nuclei in RAW264 cells. They were also not toxic to L929 cells but caused a slight deformation in the nuclear shape. Although both NPs and NWs entrapped in the cells, as seen via TEM, the cytotoxicity and genotoxicity results were completely different when the cells were directly exposed to the NPs. The chemical changes of the NPs contained in the vesicles (or cells) are a likely explanation for the obtained differences in cytotoxicity and genotoxicity because of their surface effect (large surface area per volume). If the NWs had indeed been entrapped in the cells, their extent of entrapment was negligible and, thus, they did not disrupt cell viability. However, further research is needed to fully characterize the genotoxic effects of nanomaterials toward various cell types.

## ACKNOWLEDGMENTS

A part of the study was carried out at the Research Center for Ultra-High Voltage Electron Microscopy, Osaka University. The authors are grateful to Dr. Ryusuke Kuwahara for technical support.

## REFERENCES

1. Song MM, Song WJ, Bi H, Wang J, Wu WL, Sun J, Yu M. Cytotoxicity and cellular uptake of iron nanowires. Biomaterials 2010; 31:1509–1517.
2. Ji Z, Wang X, Zhang H, Lin S, Meng H, Sun B, George S, Xia T, Nel AE, Zink JI. Designed synthesis of $CeO_2$ nanorods and nanowires for studying toxicological effects of high aspect ratio nanomaterials. ACS Nano 2012; 6:5366–5380.
3. Chen S, Goode AE, Sweeney S, Theodorou IG, Thorley A, Ruenraoengsak P, Chang Y, Gow A, Schwander S, Skepper J, Zhang JJ, Shaffer MS, Chung KF, Tetley TD, Ryan MP, Porter AE. Sulfidation of silver nanowires inside human alveolar epithelial cells: A potential detoxification mechanism. Nanoscale 2013; 5: 9839–9847.
4. Kim JM, Shin S. Toxic effects of silver nanoparticles and nanowires on erythrocyte rheology. Food Chem Toxicol 2014; 67:80–86.
5. Gao J, Xu B. Applications of nanomaterials inside cells. Nano Today 2009; 4:37–51.
6. Palomäki J, Välimäki E, Sund J, Vippola M, Clausen PA, Jensen KA, Savolainen K, Matikainen S, Alenius H. Long, needle-like carbon nanotubes and asbestos activate the NLRP3 inflammasome through a similar mechanism. ACS Nano 2011; 5:6861–6870.
7. Khang D, Liu-Snyder P, Pareta R, Lu J, Webster TJ. Reduced responses of macrophages on nanometer surface features of altered alumina crystalline phases. Acta Biomater 2009; 5:1425–1432.
8. Tripathi G, Gough JE, Dinda A, Basu B. In vitro cytotoxicity and in vivo osseointegration properties of compression-molded HDPE-HA-$Al_2O_3$ hybrid biocomposites. J Biomed Mater Res 2013; 101: 1539–1549.

9. Katsamakis S, Slot DE, Van der Sluis LM, Van der Weijden F. Histological responses of the periodontium to MTA: A systematic review. J Clin Periodontol 2013; 40:334–344.
10. Lewinski N, Colvin V, Drezek R. Cytotoxicity of nanoparticles. Small 2008; 4:26–49.
11. Kumar A, Dhawan A. Genotoxic and carcinogenic potential of engineered nanoparticles: An update. Arch Toxicol 2013; 87:1883–1900.
12. Fröhlich E. Cellular targets and mechanisms in the cytotoxicity action of nonbiodegradable engineered nanoparticles. Curr Drug Metab 2013; 14:976–988.
13. Cacchioli A, Ravanetti F, Alinovi R, Pinelli S, Rossi F, Negri M, Bedogni E, Campanini M, Galetti M, Goldoni M, Lagonegro P, Alfieri R, Bigi F, Salviati G. Cytocompatibility and cellular interaction mechanisms of $SiC/SiO_2$ nanowires. Nano Lett 2014; 14: 4368–4375.
14. Bezuidenhout M, Liu P, Singh S, Kiely M, Ryan KM, Kiely PA. Promoting cell proliferation using water dispersible germanium nanowires. PLoS One 2014; 9:e108006.
15. Xie W, Xie Q, Jin M, Huang X, Zhang X, Shao Z, Wen G. The β-SiC nanowires (~100 nm) induce apoptosis via oxidative stress in mouse osteoblastic cell line MC3T3-E1. Biomed Res Int 2014; 2014:312901.
16. Wagner AJ, Bleckmann CA, Murdock RC, Schrand AM, Schlager JJ, Hussain SM. Cellular interaction of different forms of aluminum nanoparticles in rat alveolar macrophages. J Phys Chem B 2007; 111:7353–7359.
17. Kwon JT, Seo GB, Jo E, Lee M, Kim HM, Shim I, Lee BW, Yoon BI, Kim P, Choi K. Aluminum nanoparticles induce ERK and p38MAPK activation in rat brain. Toxicol Res 2013; 29:181–185.
18. Carlson C, Hussain SM, Schrand AM, Braydich-Stolle LK, Hess KL, Jones RL, Schlager JJ. Unique cellular interaction of silver nanoparticles: Size-dependent generation of reactive oxygen species. J Phys Chem 2008; 112:13608–13619.
19. Kusaka T, Nakayama M, Nakamura K, Ishimiya M, Furusawa E, Ogasawara K. Effect of silica particle size on macrophage inflammatory responses. PLoS One 2014; 9:e92634.
20. Gliga A, Skoglung S, Wallinder IO, Fadeel B, Karlsson HL. Size-dependent cytotoxicity of silver nanoparticles in human lung cells: The role of cellular uptake, agglomeration and Ag release. Part Fibre Toxicol 2014; 11:11.
21. Studer AM, Limbach LK, Van Duc L, Krumeich F, Athanassiou EK, Gerber LC, Moch H, Stark WJ. Nanoparticle cytotoxicity depends on intracellular solubility: Comparison of stabilized copper metal and degradable copper oxide nanoparticles. Toxicol Lett 2010; 197:169–174.
22. Luo Z, Hu Y, Xin R, Zhang B, Li J, Ding X, Hou Y, Yang L, Cai K. Surface functionalized mesoporous silica nanoparticles with natural proteins for reduced immunotoxicity. J Biomed Mater Res 2014; 102:3781–3794.
23. Safi M, Yan M, Guedeau-Boudeville MA, Conjeaud H, Garnier-Thibaud V, Boggetto N, Baeza-Squiban A, Niedergang F, Averbeck D, Berret JF. Interactions between magnetic nanowires and living cells: Uptake, toxicity, and degradation. ACS Nano 2011; 5:5354–5364.
24. Studer AM, Limbach LK, Van Duc L, Krumeich F, Athanassiou EK, Gerber LC, Moch H, Stark WJ. Nanoparticle cytotoxicity depends on intercellular solubility: Comparison of stabilized copper metal and degradable copper oxide nanoparticles. Toxicol Lett 2010; 197:169–174.
25. Liu J, Hurt RH. Ion release kinetics and particle persistence in aqueous nano-silver colloids. Environ Sci Technol 2010; 44:2169–2175.
26. Kittler S, Greulich C, Diendorf J, Köller M, Epple M. Toxicity of silver nanoparticles increases during storage because of slow dissolution under release of silver ions. Chem Mater 2010; 22:4548–4554.
27. Radziun E, Wilczyńska JD, Książek I, Nowak K, Anuszewska EL, Kunicki A, Olszyna A, Ząbkowski T. Assessment of the cytotoxicity of aluminum oxide nanoparticles on selected mammalian cells. Toxicol In Vitro 2011; 25:1694–1700.
28. Simon-Deckers A, Gouget B, Mayne-L'hermite M, Herlin-Boime N, Reynaud C, Carrière M. In vitro investigation of oxide nanoparticle and carbon nanotube toxicity and intracellular accumulation in A549 human pneumocytes. Toxicology 2008; 253:137–146.
29. Di Virgilio AL, Reigosa M, de Mele MF. Response of UMR 106 cells exposed to titanium oxide and aluminum oxide nanoparticles. J Biomed Mater Res 2010; 92:80–86.
30. Kang S, Pinault M, Pfefferle LD, Elimelech M. Single-walled carbon nanotubes exhibit strong antimicrobial activity. Langmuir 2007; 23:8670–8673.
31. Chen KL, Bothun GD. Nanoparticles meet cell membranes: Probing nonspecific interactions using model membranes. Environ Sci Technol 2014; 48:873–880.
32. Uchino T, Tokunaga H, Ando M, Utsumi H. Quantitative determination of OH radical generation and its cytotoxicity induced by $TiO_2$-UVA treatment. Toxicol In Vitro 2002; 16:629–635.
33. Tsoli M, Kuhn H, Brandau W, Esche H, Schmid G. Cellular uptake and toxicity of $Au_{55}$ clusters. Small 2005; 1:841–844.
34. Gu YJ, Cheng J, Lin CC, Lam YW, Cheng SH, Wong WT. Nuclear penetration of surface functionalized gold nanoparticles. Toxicol Appl Pharmacol 2009; 237:196–204.